Numerical and mechanical modeling of the inner ear vestibular apparatus

Rony Chung, Flavio Luiz Bussamra, Pierre Selva, Joseph Morlier

NUMERICAL AND MECHANICAL MODELING OF THE INNER EAR VESTIBULAR APPARATUS

Rony T. Chung[a,b] , Flávio Luiz de S. Bussamra[a], Pierre Selva[b], Joseph Morlier[b]

[a]*Instituto Tecnológico de Aeronáutica - ITA, Praça Marechal Eduardo Gomes, 50, São José dos Campos, SP, Brazil, ronychung.br@gmail.com, http://www.ita.br/*

[b]*Département de Mécanique des Structures et Matériaux, Institut Supérieur de l'Aéronautique et de l'Espace – ISAE SUPAERO, 4 Avenue Edouard Belin, 31054 Toulouse CEDEX4, France, r.chung@isae.fr, http://www.isae.fr/*

Keywords: Inner ear, Vestibular System, Finite Elements Modeling, Computational Fluid Dynamics, Bioengineering

Abstract. As you read this text, tilt your head left and right. Note then that the text stands still. Now draw a clear line onto the ground, close your eyes and walk over it. You most likely succeeded. The aforementioned facts or abilities are remarkable skills given by a small inner ear organ set, the vestibular system. Usually operating in the background, this structure infrequently comes to the attention of our conscious mind. In this work, three finite element models (in CATIA V5R18 and COMSOL Multiphysics 3.5a environments) are developed to provide a mechanical understanding of this formidable nature's gift. In these numerical models, a fluid structure interaction modeling is presented to show the system behavior during a horizontal head spin. Finally, a physical augmented scale model is proposed, including the choice of materials and a similitude study.

1 INTRODUCTION

Sense of balance or equilibrioception can be defined as one's physiological capacity of perception of the external environment, granting movements, displacements and gestures with reasonable efficacy. The simple task of standing up right or walking on a straight line is only possible for the spatial equilibrium sense exists. From this perspective, a clear permanent mental representation of one's body in the external ambiance, conscious or unconscious, along with a prompt repertoire of motor reactions adapted to specific situations, becomes critical. The balance notion, for its turn, is a plurimodal sensorial nucleus (Roman and Thomassin, 2000) whose origins are:

- Visual, providing plastic cues for localization in space and relative velocities
- Vestibular, informing the linear and angular accelerations and the head position and inclination in relation to the gravitational axis
- Proprioceptives, describing the relative disposition of different parts of the body, their tension and accelerations. This function is remarkably effectuated by the muscles acting in the upright position and profound neck muscles output nerves.

The vestibular system becomes critical in low visibility situations, such as night or cloud non-instrumental aircraft flight. Furthermore, it provides fair interpretation of high frequency movements and a vital capacity to human quotidian life, the Vestibular-Ocular-Reflex (VOR), which refers to a reflex eye movement that allows humans to fixate the gaze at one desired object while in motion. The image is stabilized on the retina through a series of rapid eye movements in the opposite direction of the body motion. For slight head movements are present all the time, the VOR is crucial. For instance, patients with impaired VOR find it difficult to read due to normal involuntary head tremors. Pilot illusions are frequent issues in aeronautics and many of them are related to the vestibular mechanism.

For the above mentioned reasons, it may be fair enough to classify the vestibular system as acutely important for good quality of life.

2 ANATOMY AND PHISIOLOGY OF THE SEMICIRCULAR CANALS

Most animals posses a pair of inner ears disposed symmetrically in relation to the Sagittal plane (vertical plane between the eyes). These structures are relatively small, of the magnitude of millimeters. The membranous labyrinth is filled up with a Newtonian incompressible potassium rich fluid, the endolymph, crucial for the orientation process (Selva et al., 2009).
The labyrinth of the inner year is constituted of two major branches, the cochlea, a peripheral part of the auditory system, and the vestibular system, a critical equilibrioception structure. For its part, the latter is subdivided in two functional sensors: the semicircular channels and the otolith, capable of measuring angular and linear rotations, respectively.

As shown in Figure 1, there are three orthogonal semicircular canals in each inner ear: the horizontal also known as lateral or external, the posterior, also named superior, and the anterior one. In the regular head position, the horizontal canal rests horizontally in space, whilst the others remain vertical.

Specifically, only the vertical canals present a common branch linking them to the vestibule, though all canals end up in the vestibule by a dilated orifice, the ampulla, and a simple orifice. The ampulla is a swelling which contains its own hair cell sensory epithelium, the crista. The bundles of crista hair cells protrude into the ampulla interior involved by a gelatinous acellular membrane, the cupula, as represented in Figure 2. This diaphragm plays a major role as a vestibular angular acceleration detector.

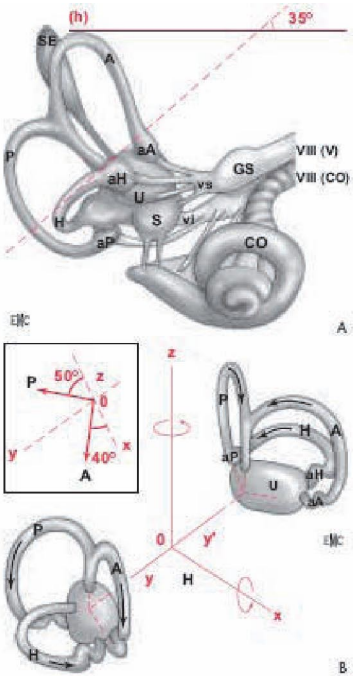

Figure 1 : Semicircular canals relative disposition (Roman and Thomassin, 2000)

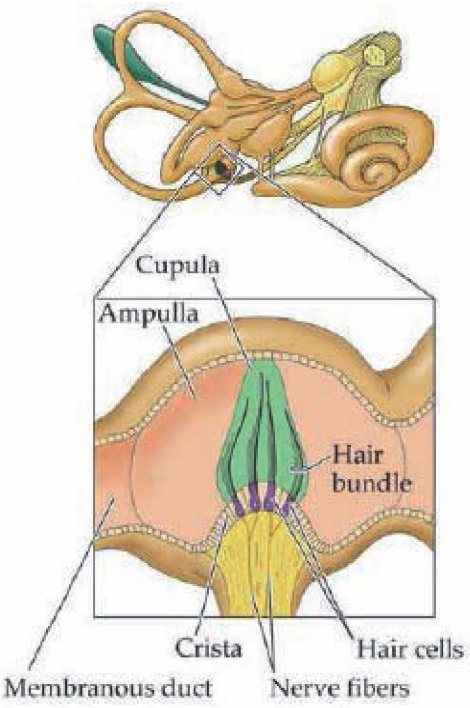

Figure 2 : Cupula Membrane (Corwin, 2006)

When there is a rotation in the horizontal plane, the horizontal semicircular canal follows. The endolymph within, however, lags behind due to its inertia, originating a relative movement between the fluid and the canal inner walls. Since the cupula is coupled to the canal, it is also in relative movement with the endolymph, which, for its part, exerts a force on the membrane, finally deflecting it. Grosso modo, each semicircular canal is predominantly excited by a pure rotation in its correspondent plan by the intersection point of the three central axes of the canals. However, during a head rotation, usually all three canals are excited because the inner year is not located exactly in the center of the head and the canals are not perfectly oriented and orthogonal. The Central Nervous System (CNS) is charged of interpreting and calibrating this experience with the perceived reality.

For both left and right canals, a deflection towards the rostral end, as shown in Figure 3, depolarizes the hair cells. Thus, during a counter clockwise rotation, a depolarization of the hair cells occurs on the left canal and a hyperpolarization takes place on the right one. Since the canals are mirror-opposite, they always operate antagonistically as push-pull pairs, or, in simple terms, when one is hyperpolarized, the other one is depolarized. Figure 3 illustrates the scheme. These signals are transmitted to the neurons that innervate the canals and are then delivered to the CNS for post-processing. Figure 4 illustrates the deformation and transduction process. A similar line can be applied to explain the posterior and anterior semicircular canals transducers.

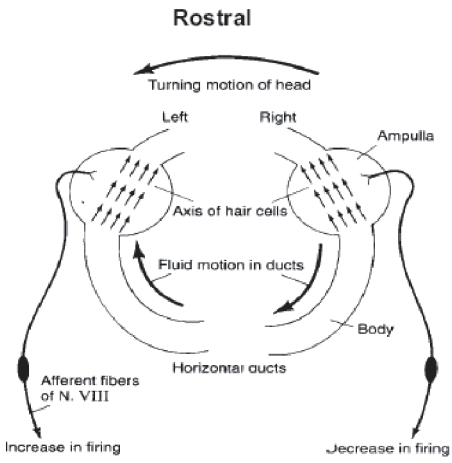

Figure 3: Canal Excitation In Both Ears (Corwin, 2006)

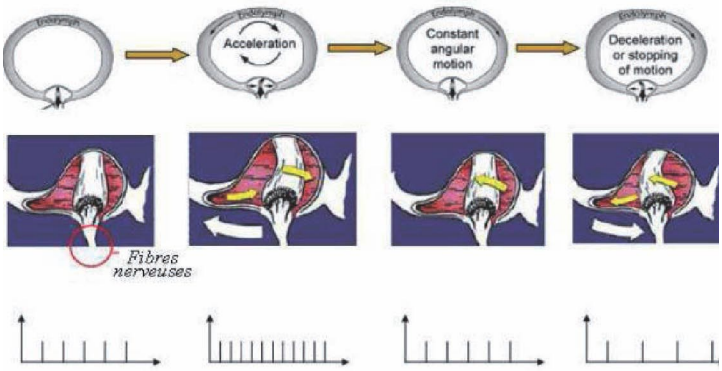

Figure 4: Cupula deformation due to Endolymph Pressure

It is important to remark, though, that once the acceleration ceases, the endolymph tends to spin along with the canal walls due to its viscosity and the non slipping condition. Moreover, the cupula gradually returns to its unstrained state due to its elastic properties, describing more precisely an exponential curve (Selva et al., 2009).

3 NUMERICAL MODEL

3.1 Fluid structure interaction

The problem must be resolved with a multiphysical algorithm, since pressure and viscous forces exerted by the fluid on the structure cause it to deform, and this deformation may significantly alter the original flow geometry. The arbitrary Lagrangian-Eulerian (ALE) method handles the geometry deformation and fluid changing boundaries with a moving grid. In this approach, the so called mesh smoothing takes place, with the computation of new mesh coordinates based on the movement of structure boundaries. The Navier-Stokes equations that solve the flow are employed in this set of moving coordinates. For its turn, the structural mechanics part of the model does not require the ALE method and is thus solved in a fixed coordinate system as usual. Nonetheless, its strains serve as feedback information for computing the deformed coordinates with ALE.

The fluid flow is derived from the incompressible Navier-Stokes equations for the velocity field $\boldsymbol{u} = (u, v, w)$. Being ρ the fluid density, η the dynamic viscosity, p the pressure and $\boldsymbol{u_m}$ the coordinate system velocity,

$$\rho \frac{\partial \boldsymbol{u}}{\partial t} - \nabla . [-p\boldsymbol{I} + \eta(\nabla \mathbf{u} + (\nabla \mathbf{u})^{\mathrm{T}})] + \rho\big((\boldsymbol{u} - \boldsymbol{u}_m).\nabla\big)\boldsymbol{u} = \boldsymbol{F} \tag{1}$$

$$-\nabla . \mathrm{u} = 0 \tag{2}$$

where $\boldsymbol{I}$ denotes the unit diagonal matrix and $\boldsymbol{F}$ the volume force on the fluid. These equations are solved referring to boundary settings such as the no-slip condition ($u = v = w = 0$) in the contact with a fixed wall, a reference pressure and velocities equal to deformation rates in the deformable solid and fluid interface. The structural strains are calculated through an elastic formulation and a nonlinear geometry formulation for the larger deformations. It is then necessary to solve

$$\rho_s \frac{\partial^2 \boldsymbol{u}_s}{\partial t^2} = \nabla . \boldsymbol{\sigma_s} \tag{3}$$

where $\boldsymbol{u}_s = (u_s, v_s, w_s)$ is the displacement vector, ρ_s is the material density and $\boldsymbol{\sigma_s}$ is the stress tensor. Considering an elastic isotropic material, the generalized Hookes law gives

$$\boldsymbol{\sigma_s} = 2\kappa\boldsymbol{\epsilon} + \lambda tr(\boldsymbol{\epsilon})\boldsymbol{I} \tag{4}$$

The coefficients μ and λ are the Lame's coefficients and can be related to the Young Modulus E and the Poisson's ratio ν through

$$\kappa = \frac{E}{2(1+\nu)} \tag{5}$$

$$\lambda = \frac{\nu E}{(1+\nu)(1-2\nu)} \tag{6}$$

As boundary conditions, the solid on the fluid solid interface is subject to a fluid pressure $\boldsymbol{F_T}$. Also, as aforementioned, the velocity field on the fluid solid interface is obtained with the deformation rate

$$\boldsymbol{F}_T = -\boldsymbol{n}.\left(-p\boldsymbol{I} + \eta(\nabla \mathbf{u} + (\nabla \mathbf{u})^{\mathrm{T}})\right) \tag{7}$$

$$\boldsymbol{u} = \frac{d\boldsymbol{u_s}}{dt} \tag{8}$$

where $\boldsymbol{n}$ denotes the boundary normal vector.The moving mesh can be computed with algorithms such as the Winslow smoothing. In this case, the solved equation system is

$$\frac{\partial^2 X}{\partial x^2} + \frac{\partial^2 X}{\partial y^2} = 0 \tag{9}$$

$$\frac{\partial^2 Y}{\partial x^2} + \frac{\partial^2 Y}{\partial y^2} = 0 \tag{10}$$

where x and y are the spatial coordinates in the frame to be the defined and X and Y are are the reference coordinates of the reference frame. At the boundaries of the solid obstacle, the mesh displacement is the same as the structural deformation. At the exterior boundaries of the flow domain, this deformation is null in all directions.

In COMSOL Multiphysics (COMSOL, 2008), which is employed in the numerical analysis in this work, the resolution is supported by three application modes which interact to solve the multiphysic problem: the incompressible Navier-Stokes for the fluid flow, the Plane Strain for the structure mechanical segment and the Moving Mesh (ALE) for computing the mesh deformation.

The computational model has been developed in COMSOL Multiphysics with the following simplifications: the model comprises the utricule and the semicircular canals with their ampullas; the saccule and other labyrinth components influence is assumed neglectful; the geometry of the semicircular canals are deemed similar and with constant elliptic section and, for geometry simplicity, the cupula is modeled in such a manner that it entirely blocks the ampulla cross-section. The model geometry was created with computer aided design (CAD) in CATIA.

3.2 Geometry

In this section, the CAD design took part in CATIA V5R18. In general terms, three models have been designed: the horizontal (single), horizontal/posterior (double) and horizontal/posterior/anterior (triple) semicircular canals models, all of which containing the utricule and ampulla cupula segment.

Firstly, the geometry of the single horizontal vestibular canal - along with the ampulla cupula – has been designed according to the dimensions shown in Figure 5. In simplified terms, the utricule cupula part has been constructed with the aid of cross sections, connected with the *Multi-sections Solid* tool. For the horizontal canal, the *nervure* tool has been used with a semicircular guide curve and an elliptic cross section. A connection root has been extruded on the utricule surface for pressure input and future link with the other canals. Also, four defined cross sections have been delimited for the cupula modeling in COMSOL.

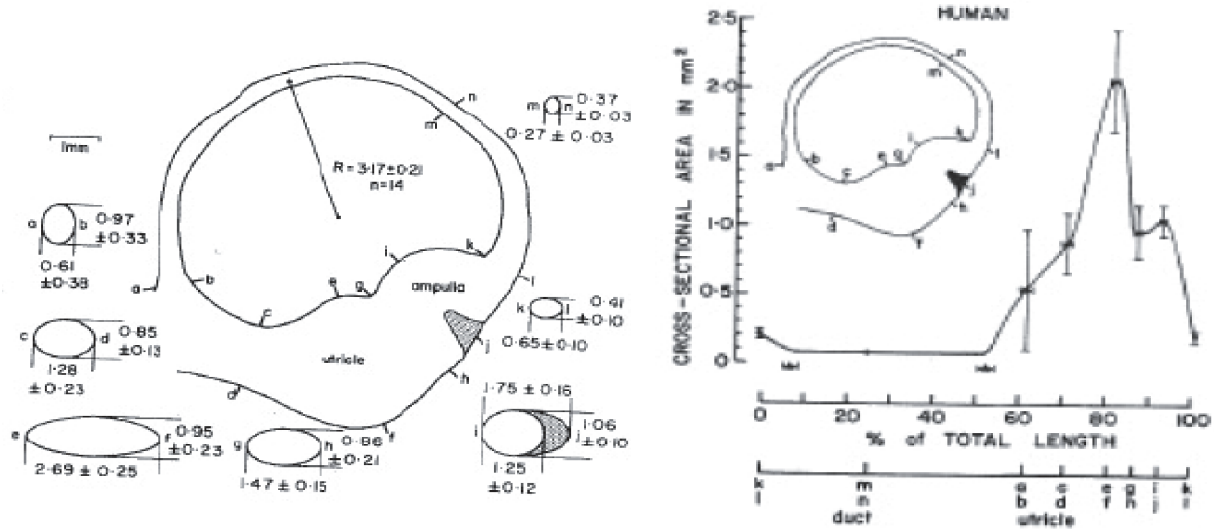

Figure 5: Horizontal Canal Geometry (Curthoys and Oman, 1987)

Should the similarity of the three semicircular canals be taken, the mentioned structure could be rotated by 90 degrees around the x and y axes to build up the anterior and posterior canals, with slight geometrical differences. The newly formed canals are connected to the utricule by a common branch.

As the main objective was the exportation to COMSOL Multiphysics, an effort has been made to construct continuous soft surface CAD geometries which the latter could eventually recognize. For this same reason, the *Boolean partial relimitation* tool has been used in the anterior and posterior canals connections to the utricule and for the common branch bifurcation. The multiphisical model is obtained from the importation of the CATIA stp format file with the COMSOL CAD Import Module.

3.3 Model Study Case

The multiphysical model consists of angular velocity imposition on the canal walls and utricule endolymph, which for its part originates pressure on the cupula diaphragm deflecting it. The walls are set to be rigid, except for the cupula adjacent regions, whose mesh is set to move freely (ALE), and the cupula (Solid Subdomain), set to deform due to endolymph pressure (Fluid Subdomain). A temporal analysis is utilized and in the post processing phase, after a horizontal head input angular velocity, the fluid velocity field and the cupula deflection

can be observed.

The tested input movement is a pure turn around the horizontal canal central normal axis. The Δ_x and Δ_y displacement and v_x and v_y velocities are given by

$$\Delta_x = [X.\cos(\omega.t) + Y.sen(\omega.t) - X] * flc2hs(t - t_0, \Delta t) \quad (11)$$

$$\Delta_y = [X.\cos(\omega.t) + Y.sen(\omega.t) - X] * flc2hs(t - t_0, \Delta t) \quad (12)$$

$$v_x = \frac{d\Delta_x}{dt} \quad (13)$$

$$v_y = \frac{d\Delta_y}{dt} \quad (14)$$

where $\omega = 0.5\, rad/s$ is the steady state angular speed and the function $flc2hs$ is used to soften the step input in angular velocity in the beginning of the simulation, avoiding problems in the derivatives v_x and v_y calculations. $t_0 - \Delta t$ and at $t_0 + \Delta t$ correspond, respectively, to the beginning and the end of the step input. In the single canal problem, $t_0 = 0.13\, s$ and $\Delta t = 0.12\, s$. For the double and triple canal models, $t_0 = 0.18\, s$ and $\Delta t = 0.16\, s$. Figure 7 and Figure 8 show the imposed angular velocities ω.

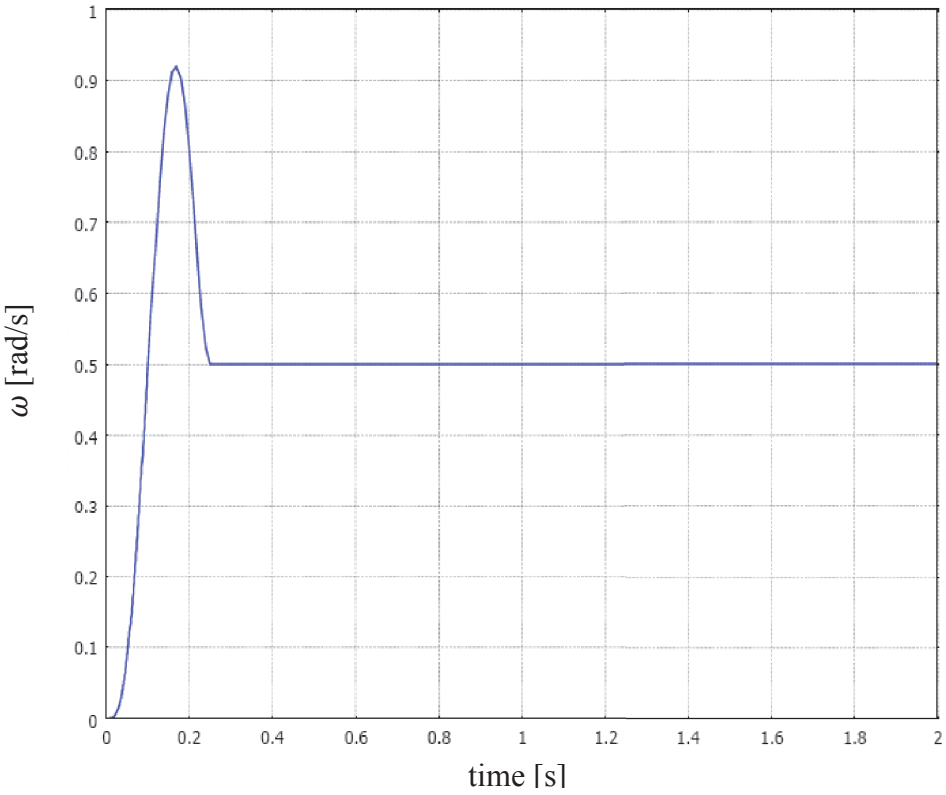

Figure 7: One Canal Input Velocity with Time

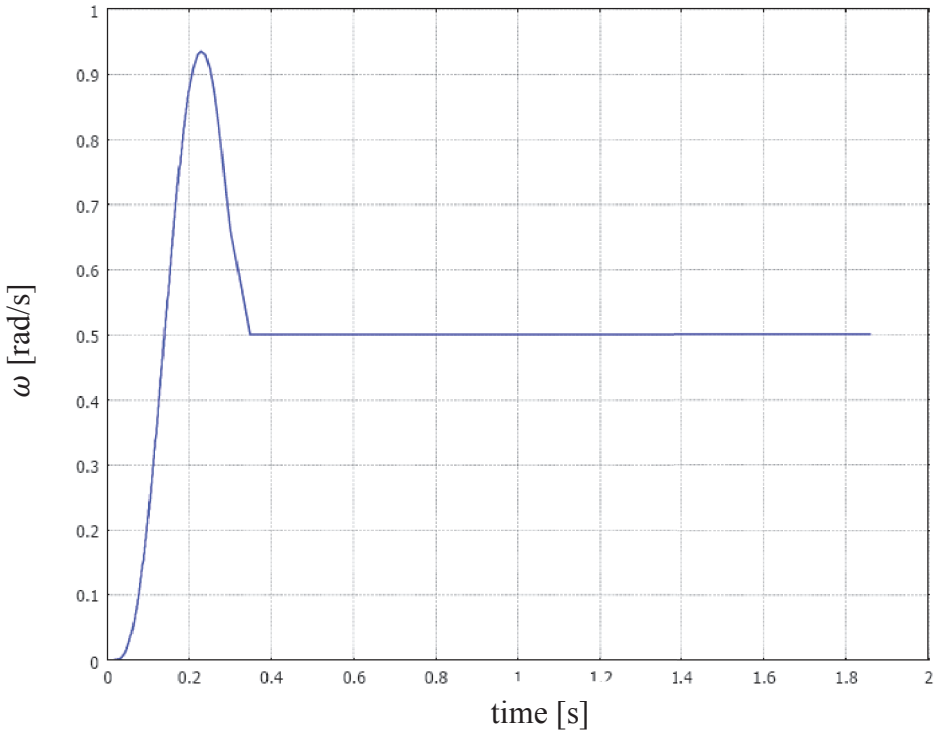

Figure 8: Double and Triple Canal Input Angular Velocity with Time

3.4 Material Properties

The Cupula is modeled as a membrane (Solid Subdomain) and the Endolymph as a fluid (Fluid Subdomain). Their pertinent utilized properties are shown below in Table 1. Those properties are applied to their respective elements after the meshing process.

Property [unit]	Symbol	Cupula	Endolymph
Young Modulus [Pa]	E	5.00	-
Kinematic Viscosity [m^2.s]	ν	-	0.33
Density [kg/m^3]	ρ	1020	1020

Table 1: Material Properties

3.5 Boundary Conditions

As the CATIA models are rigid walls closed organs, an outside reference pressure is needed as a boundary condition. For that reason, a built in entrance with a free flow condition is imposed in all three models. The fluid no-slip condition in relation to the canal walls is modeled by making the fluid boundaries spin along with the walls at the same rate. Thus, the canal walls obey Eq.(11) to Eq.(14). In the fluid solid interface, the endolymph moves at a velocity according to Eq.(8) and the cupula boundaries are finally set to face the pressure field given by Eq.(7).

3.6 Meshing

The meshing was conducted primarily with COMSOL Automatic Mesher. As the existence of small and inverted elements is hazardous for the solver convergence and calculation velocity, regions where they were present have been manually remeshed. For the

ampulla and cupula sections, a final additional refinement was implemented, not only because of the cupula membrane, but also due to the high variation in the canal cross-section and medium line, establishing special flow conditions. Tetrahedral elements have been utilized with approximately 16000, 20000 and 25000 elements for the single, double and triple canal models (see Figure 6). Later refinements were limited due to limited solving memory capacity (8 GB RAM).

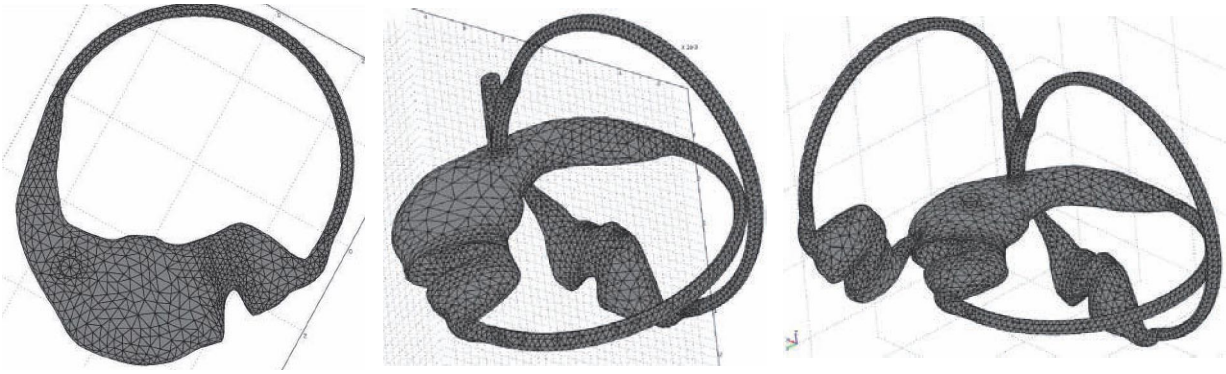

Figure 6: Model Meshed geometry configurations

3.7 Post-processing

The velocity field in the canal reference frame and the cupula deformation with time can be seen from Figure 7 to Figure 13. for each canal in the following pages. From Figure 7, it can be seen that an endolymph counterclockwise recirculation flow is established on the left side of the cupula. The Reynolds number being low due to low speed and canal dimensions, the flow is totally laminar. For $t = 0.13\ s$, the maximum input angular velocity is imposed, and thus the maximum flow speed is reached on top left side. A consequence of this flow velocity field is a higher pressure on the right side of the cupula, which results in its leftwards displacement shown in Figure 8. The maximum strain is developed in a time lag of $\Delta t_1 = 0.04\ s$ at $t_1 = 0.17\ s$.

For the double canal model (Figure 9 and Figure 10), the obtained results do not appear to fit well the real system and the achieved simulation time was short. The velocity at the free flow boundary is highest among all, edging the single canal model maximum flow speed by ten times. The originated swirl is then clockwise, probably also due to the introduction of the posterior canal, lowering locally the pressure. The flow in this case exits the semicircular canal, describes a clockwise swirl in the utricule and exits by the open boundary. This model presented some singularities in the velocity field close to the cupula free adjacent regions. The horizontal canal velocity reaches a maximum at the end of simulation $t = 0.26s$ in the semicircular canal, and the maximum strain is developed at $t_1 = 0.23\ s$.

In the triple canal model the highest velocities and strains (Figure 11) are reached in the anterior canal due to the fact that this canal's ampulla is inclined in comparison with the horizontal plane. Thus the effect of gravity pulls down the cupula and originates a higher upper flow pressure on the membrane, deflecting it downwards . On the other hand, the flow in the posterior canal is not as intense, as one would expect from a pure horizontal rotation stimulus. For better viewing the horizontal canal, Figure 12 and Figure 13. omit the anterior canal results. It can be seen that, for $t = 0.198\ s$, the maximum horizontal canal velocity is obtained and after $\Delta t_1 = 0.202\ s$, or $t_1 = 2.200\ s$, the maximum displacement is obtained. It is interesting to note that, because of gravity, the maximum velocity is now situated on the

outfall of the posterior canal into the horizontal one, but is in magnitude similar to the one canal model. Also, this flow results in a final horizontal cupula in one order of magnitude higher.

4 SCALE MODEL

The objective of this part was constructing a physically similar augmented model of one semicircular canal and the utricule for both quantitative and qualitative testing. Price, construction simplicity and material availability have been determinant variables during this project. The project requirements are listed: size of the model large enough to be easily observed and photographed during the experiments. This restraint could be translated as a minimum scale factor of 20, considering the small dimensions of the vestibular system (around 7mm long). On the other hand, its scale should also be limited superiorly by 100; transparence of the fluid representing the endolymph, due to the visual experiments; low manufacturing complexity; reasonable price; cupula Material Young Modulus non inferior to $E'_{minimum} = 0.005\ GPa$ (silicone rubber). Equally, for the tests: maximum Scale Model angular velocity limited by $\omega'_{max} = 250°/\text{s}$, due to equipment restraints; minimum Simulated Angular Velocity of $\omega_{min} = 10°/\text{s}$.

4.1 Similitude Analysis

The fabrication of the scale model was preceded by a Similitude Study, with the use of the Buckingham Pi theorem (Dym, 2004), in order to verify the materials required properties and thus their feasibility in the project. The dimensionless numbers theory shall then be derived. Given the fundamental units M(mass), L (length) and T (time), the physical parameter G_i may be written as

$$G_i = L^{a_1} M^{b_1} T^{c_1} \tag{10}$$

where α_1, α_2 and α_3 are integer coefficients. More specifically,

Fluid density: $G_1 = \rho = \frac{M}{L^3}$	Angular velocity: $G_4 = \omega = \frac{1}{T}$
Cross section radius: $G_2 = r = L$	Cupula Young Modulus: $G_5 = E = \frac{M}{LT^2}$
Dynamic viscosity: $G_3 = \mu = \frac{M}{LT}$	Canal length $2\pi R$: $G_6 = l = L$

Table 2: Physical parameters dimensional analysis

The fluid velocity is function of

$$\dot{y} = f(\rho, r, \mu, E, \omega, l) = L^x M^y T^z = \frac{L}{T} \tag{11}$$

$$x = 1;\ y = 0;\ z = -1 \tag{12}$$

In terms of the physical properties, the velocity can be expressed as

$$\dot{y} = G_1^{\alpha_1} G_2^{\alpha_2} G_3^{\alpha_3} G_4^{\alpha_4} G_5^{\alpha_5} G_6^{\alpha_6} \tag{13}$$

Substituting the expressions in Table 2 in Eq.(13) is derived from the correspondent linear system:

$$\begin{cases} -3\alpha_1 + \alpha_2 - \alpha_3 - a_5\alpha_5 + a_6\alpha_6 = 1 \\ \alpha_1 + \alpha_3 + a_5 = 0 \\ -\alpha_3 - \alpha_4 - 2a_5 = -1 \end{cases} \tag{14}$$

Finally,

$$\dot{y} = \frac{\mu}{\rho r}\left(\frac{\rho r^2 E}{\mu^2}\right)^{\alpha_5}\left(\frac{\rho r^2 \omega}{\mu}\right)^{\alpha_4}\left(\frac{l}{r}\right)^{\alpha_6} \tag{17}$$

$$\dot{y} = \frac{\mu}{\rho r} f\left[\left(\frac{\rho r^2 E}{\mu^2}\right), \left(\frac{\rho r^2 \omega}{\mu}\right), \left(\frac{l}{r}\right)\right] \tag{18}$$

It is therefore required to keep constant the three dimensionless numbers in Table 3, in order to pursuit physical similitude:

Dimensionless Number	Comments
$\left(\frac{l}{r}\right)$	This geometrical relation can be easily maintained by adjusting the correct canal length to a chosen cross-section radius.
$\left(\frac{\rho r^2 E}{\mu^2}\right)$	The main restraint of the scale model problem resides in maintaining this second dimensionless number, because it requires an extremely low Young Modulus for the model Cupula Material.
$Re = \left(\frac{\rho r^2 \omega}{\mu}\right)$	The third dimensionless number is the Reynolds number, in this case expressed in terms of angular velocity.

Table 3: Dimensionless numbers description

Let the scale model variables are referred with an apostrophe. Thus, if r means the inner ear cross-section radius, r' represents the scale model cross-section radius. The scale factor A exists so that $r' = Ar$ is the new cross section radius. For conserving the second dimensionless number, it may be written

$$\left(\frac{\rho r^2 E}{\mu^2}\right) = \left(\frac{\rho' r'^2 E'}{\mu'^2}\right) \tag{19}$$

From which

$$E' = \left(\frac{\mu'}{A\mu}\right)^2 \left(\frac{\rho}{\rho'}\right) E \tag{20}$$

Given that

$$\nu = \frac{\mu}{\rho} \tag{21}$$

The Young Modulus expression assumes the form

$$E' = \left(\frac{\nu'}{A\nu}\right)^2 \left(\frac{\rho'}{\rho}\right) E \tag{22}$$

By naming the linear coefficient

$$k = \left(\frac{\nu'}{A\nu}\right)^2 \left(\frac{\rho'}{\rho}\right) \tag{23}$$

We have

$$E' = k.E \tag{24}$$

The main limitation of the problem is that E is considerably small, namely $E \sim 5\ Pa$. For this reason, the coefficient k has to be large enough so that $E' = k.E \geq E_{minimum}$. In a practical approach, the density ρ' and the scale factor A play a minor role in influencing k, as they don't vary much in magnitude as ν' does (ρ' values are generally the same order of magnitude of water density and $20 \leq A \leq 100$ is a project requirement).ν' values, for their part, vary in range length superior to 10^8units. For solving this Cupula Material limitation, then, it is essential that the model fluid kinematic viscosity ν' be high, so that E' does surpass $E'_{minimum}$.

As long as $Re = Re'$, by choosing a large enough value for ν', ω is relatively larger than ω' in a scale model experiment when all other variables are kept constant. In other words, the simulation of a chosen head rotation requires an even larger scale model rotation. This fact can be shown by

$$Re = Re' \tag{25}$$

$$\left(\frac{\rho r^2 \omega}{\mu}\right) = \left(\frac{\rho' r'^2 \omega'}{\mu'}\right) \tag{26}$$

Obtaining the simulated angular velocity

$$\omega = \left(A^2 \frac{\mu \rho'}{\mu' \rho}\right) \omega' \tag{27}$$

Or

$$\omega = \left(A^2 \frac{\nu}{\nu'}\right) \omega' \tag{28}$$

As ω' is superiorly limited by equipment restraints, Eq.(28) shows that ν' cannot be as large as desired, otherwise the project criterion $\omega \geq \omega_{min}$ would not be met. As aforementioned, ν' should be, though, large enough due to the restraint $E' \geq E'_{minimum}$. Concluding, a balance value for ν' must be established so that both specifications are obeyed. A larger value for A aids less substantially in the rotation problem, but shall be considered in a second analysis.

4.2 Materials Choice

For modeling the endolymph, the Polydimethylsiloxane Silicone Oil has been chosen for representing high enough Cupula elasticity modulus, providing experiments with higher rotational rates. Equally, the commercial easiness to find it renders it an attractive choice. The silicone rubber presents other interesting features, to mention: clear, colorless, odorless, fluid; extremely high kinematic viscosities, covering a wide range; little viscosity change with temperature; high temperature stability and high oxidation resistance. It shall also be pointed that the mentioned fluid covers a wide range of possible kinematic viscosities (from less than

0.65 till 20 million cSt), whilst maintaining practically constant density (978 kg/m^3).

For the Cupula, low elasticity modulus silicone rubbers, with $E' \sim E_{minimum} = 0.005\ GPa$ have been considered, for highly elastic materials are required for high viscosity fluids. By choosing the material's lowest possible Young modulus, lower part of high kinematic viscosities ν' can be utilized, minimizing the rotation ratio limitation.

The vestibular canal walls can be modeled with transparent flexible plastic hoses, a simple and low-cost solution.

4.3 Sample Proposed Simulations

For the largest scale factor, $A = 100$, the expression $\omega = \left(A^2 \frac{\nu}{\nu'}\right)\omega'$ allows the construction of Table 4, with sample construction possibilities and their respective simulated speeds. A set of experiments could also be determined, depending on the availability of the materials in the market and their price, and as a result, the chosen fluid cinematic viscosity was $\nu' = 60{,}000\ cSt = 0{,}06\ m^2/s$ (*Wacker® AK 60,000 cSt Silicone Oil*). The suggested cupula silicone rubber can be the *Smooth-On Ecoflex 00-10*, a mold making material whose Young Modulus is close to the required. It is composed of a base and a catalyst that must be mixed and cured to mold the silicone rubber in desired shape.

Polydimethylsiloxane and A = 100				
ν' (m²/s)	0,03	0,05	0,06	0,07
E' (GPa)	0,001	0,003	0,005	0,006
ω (°/s)	ω' (°/s)	ω' (°/s)	ω' (°/s)	ω' (°/s)
10	35,3	58,8	70,6	76,5
15	52,9	88,2	105,9	114,7
20	70,6	117,6	141,2	152,9
25	88,2	147,1	176,5	191,2
30	105,9	176,5	211,8	229,4
35	123,5	205,9	247,1	267,6
40	141,2	235,3	282,4	305,9
45	158,8	264,7	317,6	344,1
50	176,5	294,1	352,9	382,4
55	194,1	323,5	388,2	420,6
60	211,8	352,9	423,5	458,8
65	229,4	382,4	458,8	497,1
70	247,1	411,8	494,1	535,3
75	264,7	441,2	529,4	573,5
80	282,4	470,6	564,7	611,8
85	300,0	500,0	600,0	650,0
90	317,6	529,4	635,3	688,2

Table 4: Possible experiments. Highlighted cells indicate cases where the minimum project simulated velocity $\omega_{\min} = 250°/s$ is met

5 CONCLUSION

The numerical finite element model provides a visual understanding of the cupula response to external stimulus. It has been seen that the flows highest speeds take place in a flow

recirculation region illustrating the pressure mechanism with which the endolymph exerts a force due to the fluid pressure difference on both sides of the membrane. If the single canal model functioned well, the double canal model presented singularities that may render its results dubious. For the triple canal model, the anterior semicircular canal presented a great difference in the model conception for being greatly influenced by gravity.

For future works regarding the vestibular modeling problem, one may leave as a suggestion for different FEM models the elaboration of triple canal geometry where the ampulla/cupula region of the anterior canal be in an horizontal position. This would present better results for analyzing the deflection of this membrane due to a pure horizontal rotation. Furthermore, a model can have an improved realism by modeling the cupulas as not entirely obstructive in the ampullas' endolymph flow. It would indeed provide interesting results by eliminating one boundary fixed constraint for the diaphragm structure and allowing a communication between the left and right side of the flow.

The parametric study for choosing the best materials for the augmented scale model was successfully conducted and provided satisfactory results regarding simplicity, prices and physical similitude. It will be of great value for future visual experiments.

REFERENCES

COMSOL: Model Gallery - Fluid Structure Interaction, COMSOL Web Site. November 3, 2008. http://www.comsol.com/ (accessed July 20, 2009).

Corwin, J., The Vestibular System. University of Virginia Web site. February 2, 2006. http://www.healthsystem.virginia.edu/internet/corwin-lab/educationresearch/handouts/the-vestibular-system-2006-jtc-final.pdf (accessed April 20, 2009).

Curthoys, I.S., and C.M. Oman, Dimensions of the horizontal semicircular duct, ampulla and utricule in the human. Acta Otolaryngol, 1987.

Dym, C.L, Principles of Mathematical Modeling. Burlington: Elsevier Academic Press, 2004.

Roman, S., and J.M. Thomassin, Physiologie Vestibulaire. In Encyclopédie Médico-Chirurgicale. Paris: Editions Scientifiques et Médicales Elsevier SAS, 2000.

Selva, P., Y. Gourinat, and J. Morlier, A Matlab/Simulink model of the inner ear angular accelerometers sensors. 22nd Biennial Conference om Mechanical Vibration and Noise. San Diego: ASME, 2009.

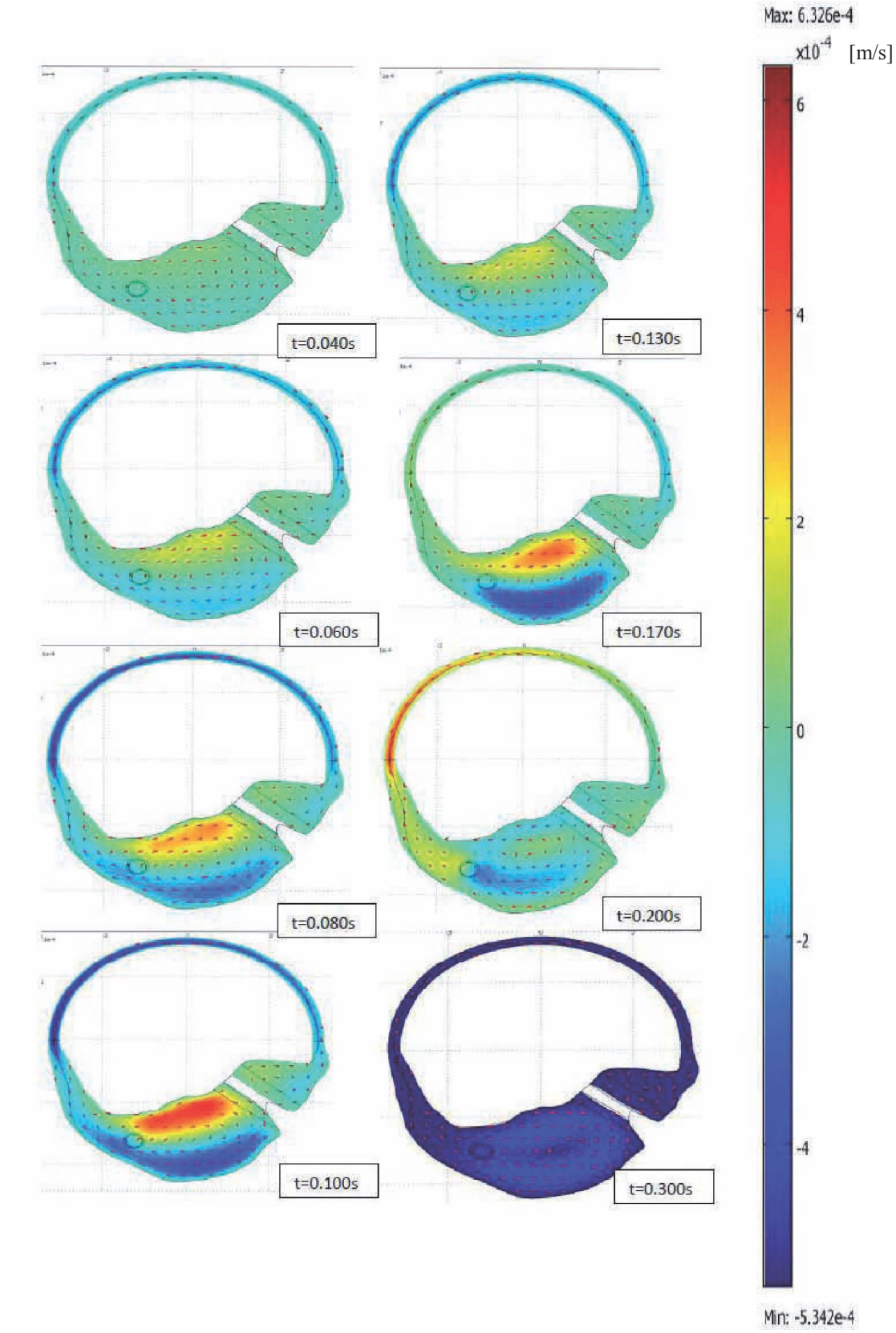

Figure 7: Single canal velocity field in organ reference frame

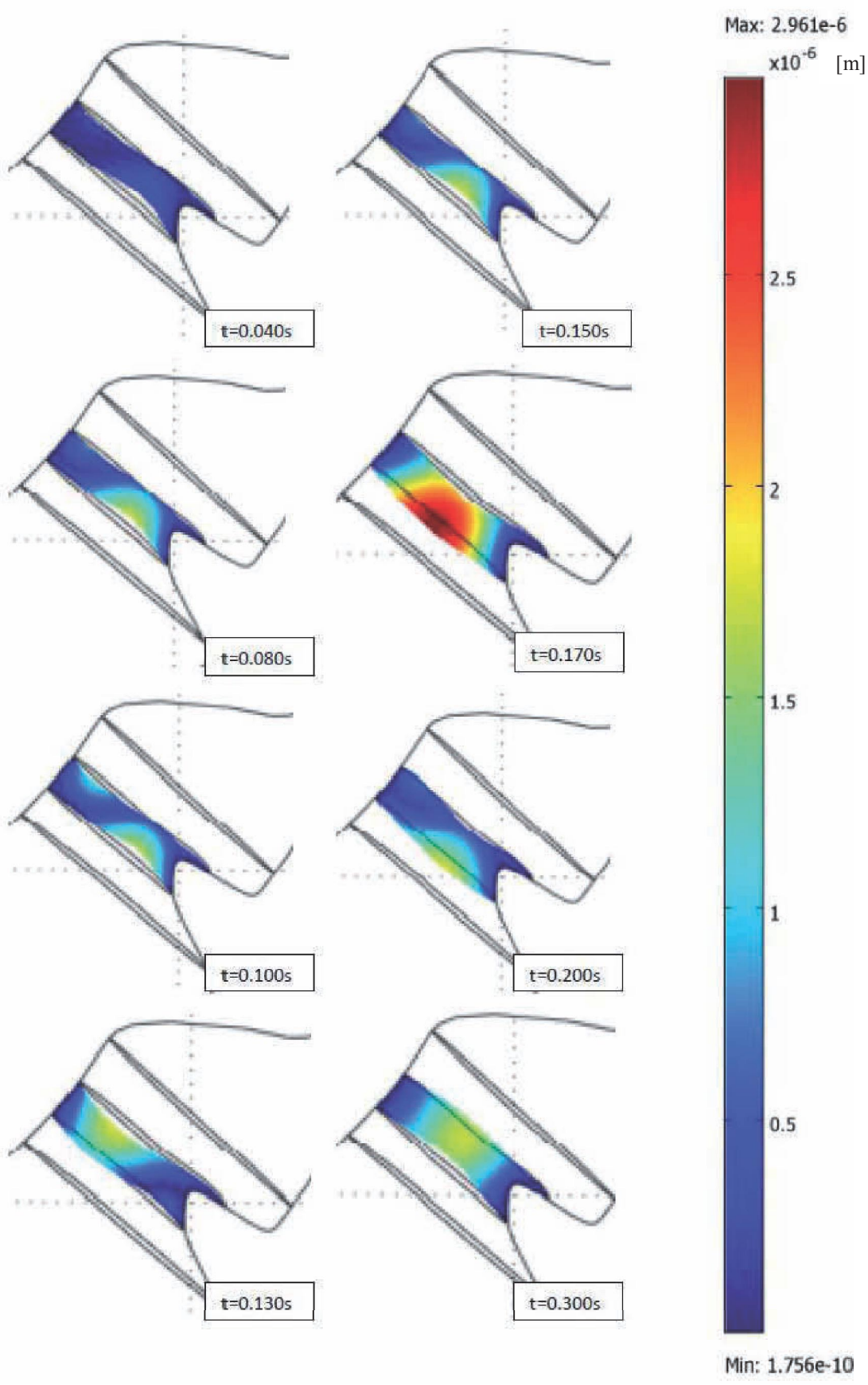

Figure 8: Single canal cúpula displacement

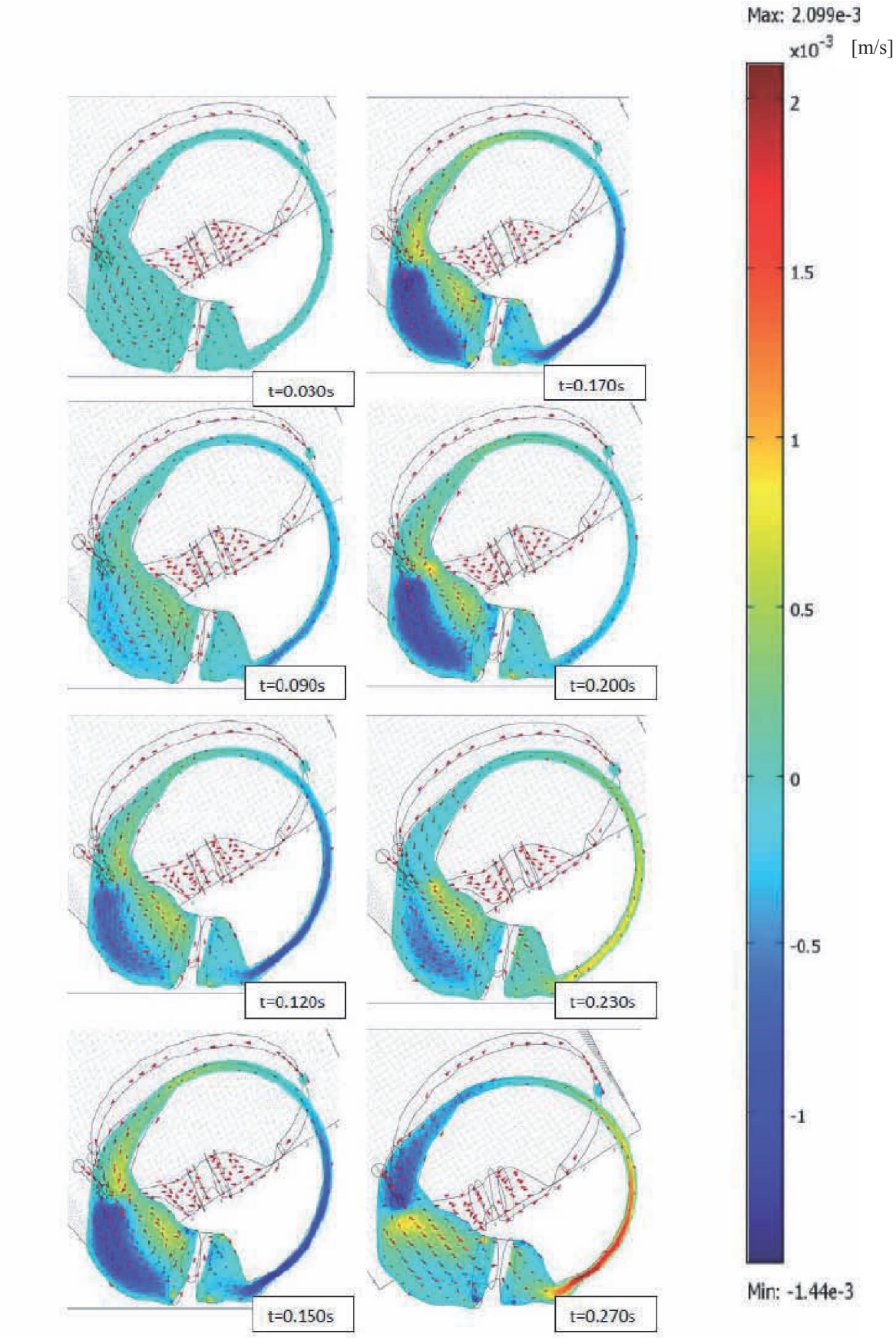

Figure 9: Double canal model velocity field in organ reference frame

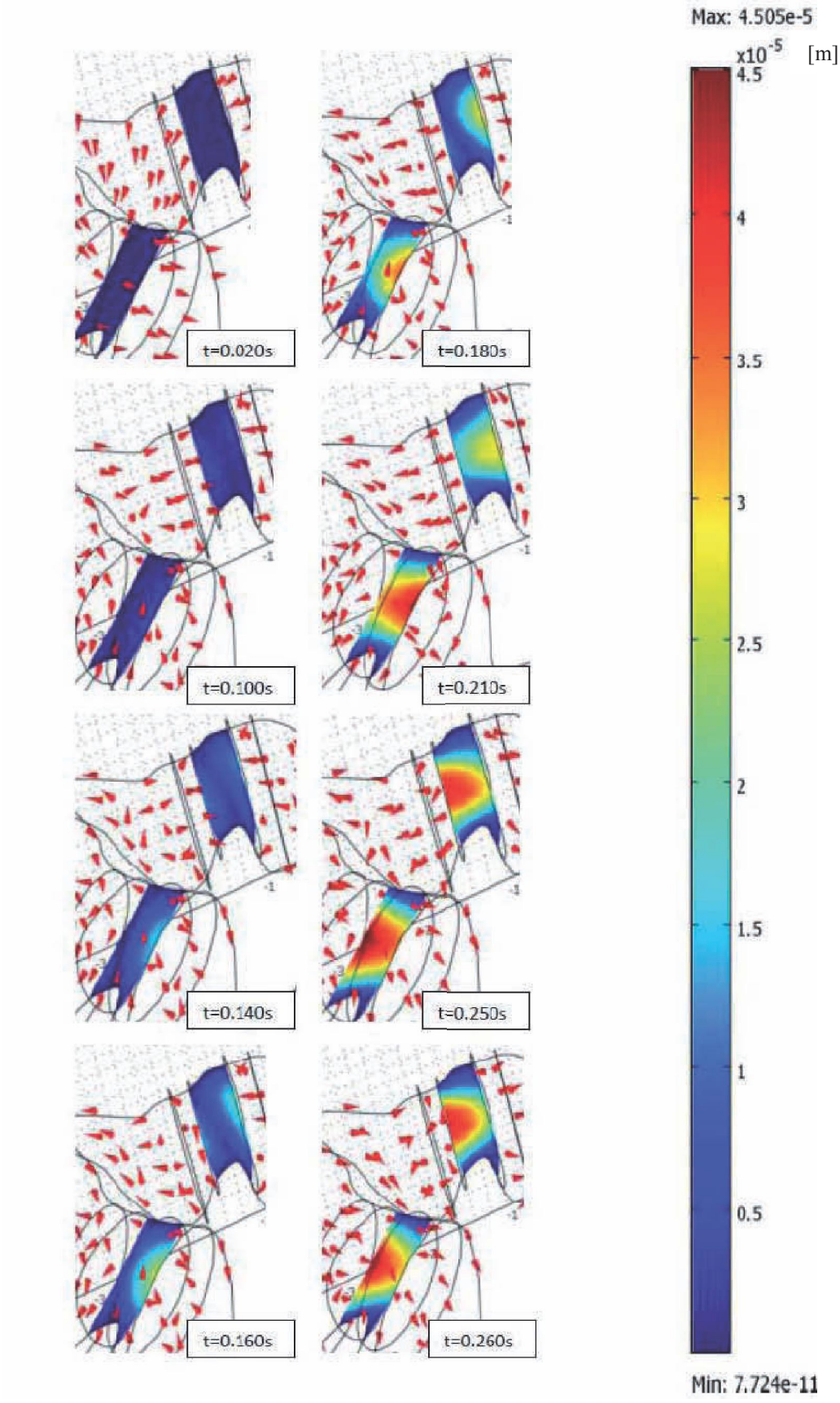

Figure 10: Double canal cupula displacement

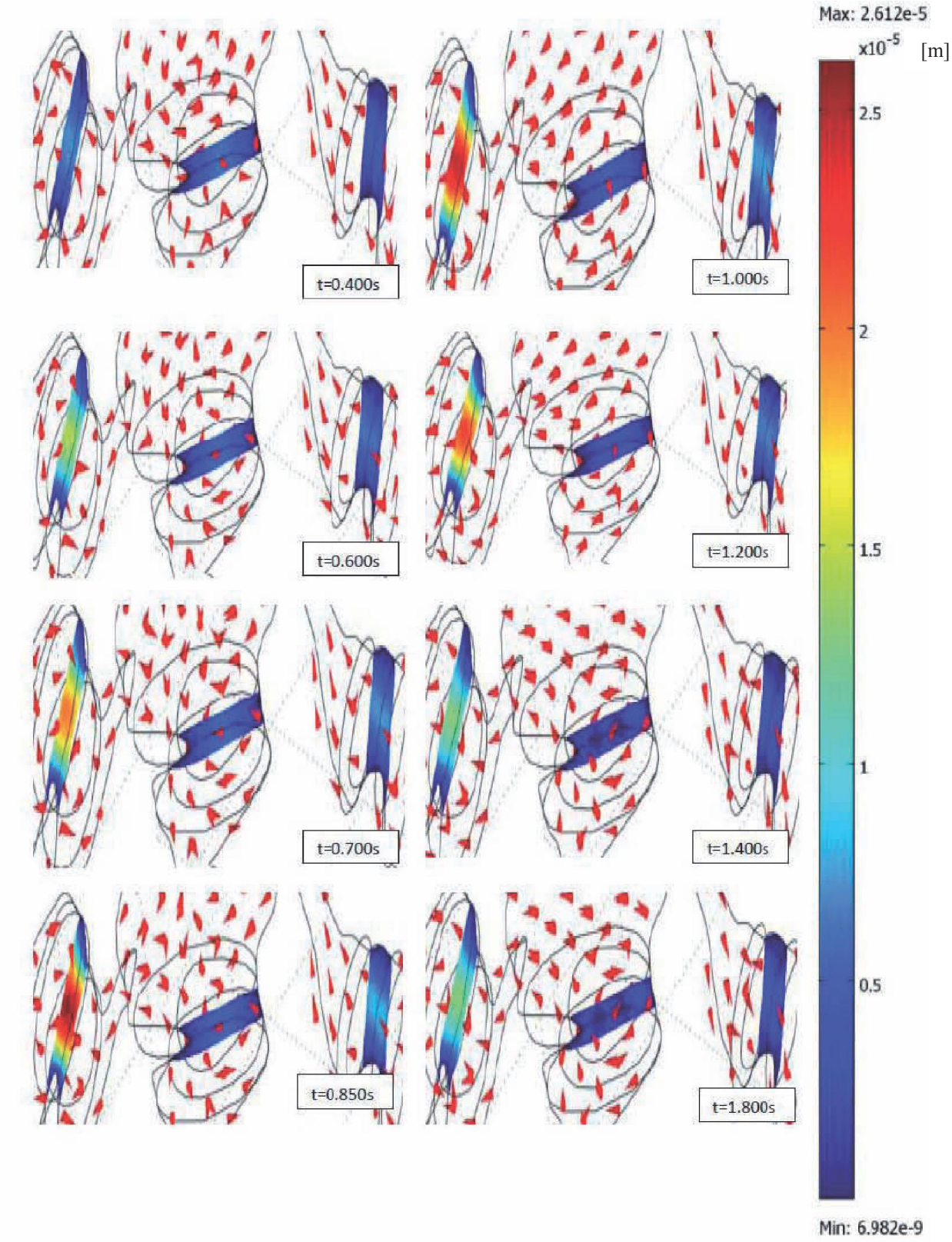

Figure 11: Triple canal cupula displacement with posterior canal

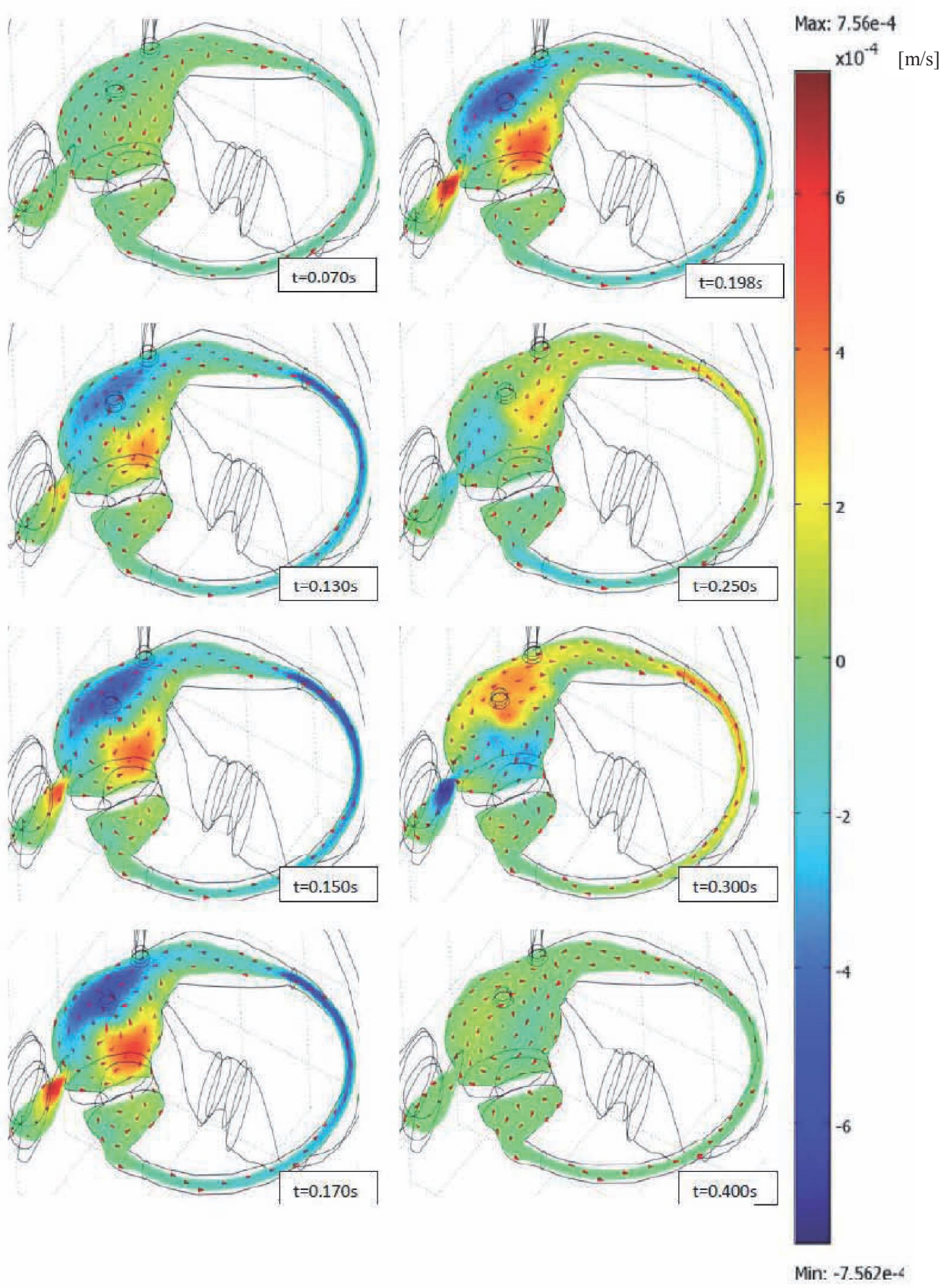

Figure 12: Triple canal velocity field in organ refrence frame

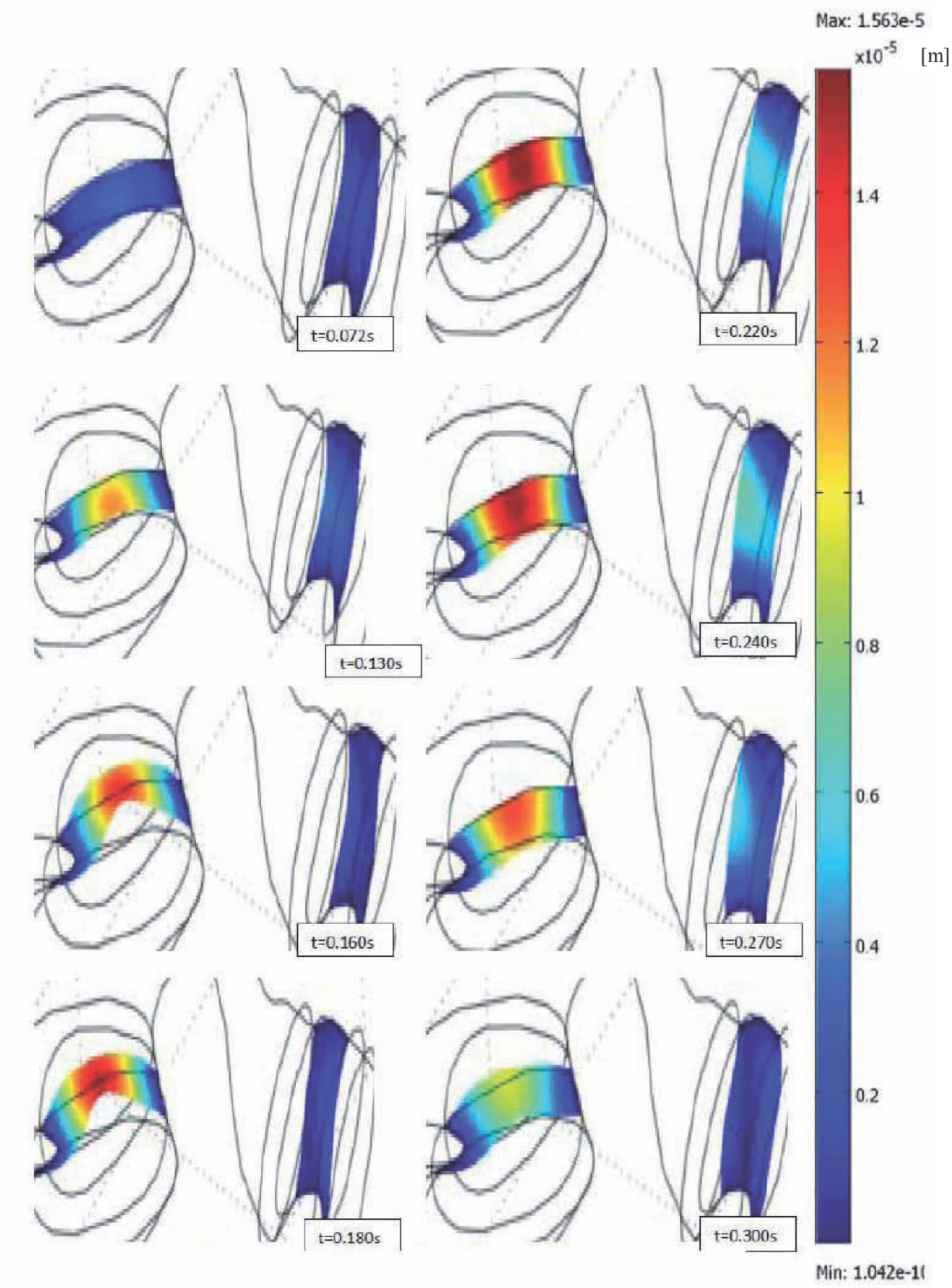

Figure 13: Triple canal cupula displacement